# Measurement of cerebral blood volume with subtraction three-dimensional functional CT.

L M Hamberg, G J Hunter, D Kierstead, E H Lo, R Gilberto González and G L Wolf

*AJNR Am J Neuroradiol* 1996, 17 (10) 1861-1869
http://www.ajnr.org/content/17/10/1861

# Measurement of Cerebral Blood Volume with Subtraction Three-dimensional Functional CT

Leena M. Hamberg, George J. Hunter, Diane Kierstead, Eng H. Lo, R. Gilberto Gonzá lez, and Gerald L. Wolf

**PURPOSE:** To implement a three-dimensional subtraction functional CT technique to permit rapid quantitative mapping of regional cerebral blood volume (CBV). **METHODS:** The 3-D functional CT technique was implemented in a rabbit model using normal and ischemic animals. Two spiral data acquisitions were performed, one before and one during biphasic administration of contrast material. CBV maps were then produced on a voxel-by-voxel basis through the whole brain. **RESULTS:** The average normal CBV was 3.3 ± 0.4 mL/100 g (n = 7), and the regional values were 4.5 ± 0.6 mL/100 g for cortical gray matter, 2.5 ± 0.6 mL/100 g for white matter, and 3.7 ± 0.4 mL/100 g for the basal ganglia. The CBVs in ischemic regions were 1.5 ± 0.4 mL/100 g, 0.7 ± 0.7 mL/100 g, and 1.8 ± 0.9 mL/100 g, respectively. **CONCLUSION:** Subtraction 3-D functional CT is a fast, potentially cost-effective method with which to assess whole-brain CBV. Because the data collected in 3-D functional CT imaging also can be used to produce large-vessel angiograms, its use in a clinical setting can provide a multiparametric study of cerebrovascular abnormalities that encompasses both large and small vessel circulations for patients being examined for stroke.

**Index terms:** Animal studies; Blood volume; Computed tomography, three-dimensional

*AJNR Am J Neuroradiol* 17:1861–1869, November 1996

The introduction of modern spiral computed tomography (CT) has substantially increased the utility of CT as a tool for demonstrating cerebrovascular insult (1–4). Most recently, spiral CT technology has been used to obtain functional studies of cerebrovascular physiology (5). These high-resolution (≤1 $mm^3$ voxel size) functional CT techniques can show cerebral perfusion and its alteration under pathophysiological conditions through the use of quantitative maps of cerebral blood volume (CBV), cerebral blood flow, and tissue transit times (5).

Because cerebral ischemia is caused by a reduction in local or general blood flow, its earliest occurrence is best demonstrated on the basis of altered cerebrovascular physiology rather than by indirect or secondary morphologic criteria. For this reason, functional applications of spiral CT have the potential to serve as effective tools in the clinical diagnosis of acute stroke, and ultimately may facilitate the rapid implementation of new treatment strategies. In this investigation, our immediate objective was to implement a three-dimensional functional CT technique, based on image subtraction and the indicator dilution principle, in an animal model so as to obtain quantitation of regional CBV. Our findings demonstrated the functionality of 3-D functional CT in normal brain and its feasibility as a tool for the study of acute cerebral ischemia.

## Materials and Methods

The 3-D functional CT technique for determining CBV was implemented in a rabbit model with seven healthy and three ischemic animals. The 3-D functional CT study consisted of two spiral CT data collections, obtained before and during the infusion of a radiopaque contrast agent. From these data, absolute regional blood volume distribution in the brain was calculated and presented in blood volume maps.

Received March 7, 1996; accepted after revision June 26.

From the Department of Radiology, Center for Imaging and Pharmaceutical Research, Massachusetts General Hospital, Boston.

Address reprint requests to Leena M. Hamberg, PhD, Department of Radiology, Center for Imaging and Pharmaceutical Research, Massachusetts General Hospital, 2nd Floor, Room 2329, Bldg 149, 13th Street, Charlestown, MA 02129.

AJNR 17:1861–1869, Nov 1996 0195-6108/96/1710–1861

*Animal Model*

Animal studies were conducted under the guidelines of our Institutional Subcommittee on Research Animal Care. Anesthesia was induced in seven normal New Zealand white rabbits (2.5 to 3.5 kg) by intramuscular injection of a mixture of ketamine (40 mg/kg) and xylazine (5 mg/kg) and was maintained by hourly injections. The femoral vein was catheterized for administration of contrast agent. Iohexol was used for all studies.

Focal ischemia was induced by effecting unilateral occlusion of the middle cerebral artery in three animals. Tracheostomies were performed and the animals were artificially ventilated with 1% to 2% halothane in a 10:1 air/oxygen mixture, with a stroke volume of 30 to 40 mL at about 20 strokes per minute. Spontaneous respiration was eliminated via immobilization with pancuronium bromide (0.2 mg/kg intravenous). Focal cerebral ischemia was induced by using a standard technique, as previously described (6). Briefly, unilateral globe enucleation was achieved with electrocautery, and a craniotomy adjacent to the optic foramen was performed under a stereomicroscope. A transorbital occlusion of the left internal carotid artery, distal middle cerebral artery, and distal anterior cerebral artery was performed via electrocoagulation. Three-dimensional functional CT imaging was performed 3 hours after occlusion. The 3-hour time interval was chosen because our previous studies with this same animal model have shown that ischemic deficits have stabilized by 3 to 4 hours after occlusion (6–8). The aim of the present work was not to study ischemia per se but to use an ischemic brain to demonstrate the potential of our subtraction 3-D functional CT technique to measure ischemia.

*Three-dimensional Functional CT Imaging Protocol*

Imaging was performed on a nutate/rotate whole-body spiral CT scanner (Toshiba, Tokyo, Japan). The anesthetized animal was placed supine in the gantry of the scanner, its position secured, a lateral scout image obtained, and the extent of the spiral path through the brain prescribed. Imaging parameters included 120 kV X-ray tube voltage, 150 mA tube current, and high-resolution imaging mode. A 1- or 2-mm section thickness, 80- or 120-mm field of view, and 512 × 512 image matrix yielded 0.024-$mm^3$ or 0.049-$mm^3$ voxels. Two separate spiral data acquisitions were performed by continuous, unidirectional rotation of the X-ray tube around the object and simultaneous cranial translation of the table at a 1:1 pitch (a speed of 1 or 2 mm/s depending on the section thickness). To obtain continuous volume along a helical X-ray trajectory through the brain, reconstruction section spacing was set equal to section thickness.

The first spiral data acquisition was done before the contrast material was administered. During the second spiral data acquisition, the contrast agent was administered via a continuous, biphasic infusion into the femoral vein with an infusion pump (Model 940, Harvard Apparatus, Natick, Mass). The first 20-second phase began before the start of image acquisition at an infusion rate of 35 mL/min. Within this time, the blood iodine concentration reached a level that caused clearly detectable attenuation of the X-rays. The infusion rate was then decreased to a value of 12 mL/min to keep the blood concentration constant during the second spiral data acquisition, which was initiated immediately thereafter. The second infusion phase was maintained until the end of scanning. After the imaging studies were complete, all animals were killed with an overdose injection of pentobarbital.

*Data Analysis*

On the basis of the contrast agent's dilution in the intravascular space, we determined the tissue blood volume fraction by measuring the change in Hounsfield units (linearly proportional to the concentration of the contrast agent) in brain tissue ($\Delta HU_{brain}$) and blood ($\Delta HU_{blood}$) and then calculating the ratio of these values. This fractional voxel blood volume was then converted to the percentage blood volume (% CBV) as well as to absolute blood volume (mL/100 g of tissue) in the following manner:

$$1)\qquad \%CBV = 100 \cdot \frac{\Delta HU_{brain}}{\Delta HU_{blood}}$$

This can be expressed in mL/100 g of tissue as follows:

$$2)\qquad CBV = \frac{\Delta HU_{brain}}{\Delta HU_{blood}} \cdot V_{voxel} \cdot N$$

where $V_{voxel}$ is voxel volume in milliliters and N is the calculated number of voxels in 100 g of tissue (N = 100 $g/V_{voxel}$ expressed in grams). A value of 1.05 g/mL for the cerebral tissue density was used (9). This is possible because the blood-brain barrier prevents contrast agent from escaping the circulation, and thus calculated signal changes may truly be localized to the intravoxel vasculature. The CBV values were also corrected for the small- to large-vessel hematocrit ratio of 0.85 (see detailed explanation in the Appendix; the 0.85 measure was taken from the study by Phelps et al [10]).

To achieve these steps, we first converted the measured signal intensity values (HU) to the changes in HU (ΔHU) by subtracting the baseline images from the contrast (infusion) images on a voxel-by-voxel basis. These calculated ΔHU images were then used for further analysis. For the seven healthy animals, we determined the average percentage of CBV for the whole brain by first drawing a region of interest (ROI) that covered the whole brain on the calculated ΔHU images. Large vessels were carefully excluded from the brain tissue ROI by thresholding in the following manner. First, a histogram of the ΔHU values was obtained from the area where the ROI was drawn. By interactively changing the selected ΔHU value in the histogram, all voxels corresponding to that value could be highlighted in the image. The ΔHU value corresponding to the outer edges of major vessels was noted and was used to threshold the brain tissue ROI to that value so as to exclude the major vessels and yield an ROI solely from the

brain tissue. The mean ΔHU value for this ROI was then obtained. Regional analysis was performed by drawing ROIs that corresponded to cortical gray matter, white matter, and basal ganglia, with the major vessels excluded from the analysis.

To avoid invasive blood sampling during the study, the iodine concentration in the blood was determined from the images according to the following technique. First, the blood ΔHU value for each animal was obtained by placing ROIs over the major intracranial vessels. To ensure that only the blood vessels were sampled, and thus to avoid partial volume effects from the surrounding brain tissue, techniques similar to the thresholding described above were used. The mean ΔHU value for the blood ROI was then determined, and the %CBV values for whole brain, gray matter, white matter, and basal ganglia were then calculated, corrected with the small-to-large vessel hematocrit ratio, and converted to CBV values expressed in milliliters of blood per 100 g of cerebral tissue, as described above (Equations 1 and 2).

The fractional blood volume maps were produced by dividing each ΔHU image by the blood ΔHU value (Equation 1). These resulting maps show the fractional blood volume distribution in the brain. Fractional blood volume maps can easily be converted to absolute blood volume maps by multiplying them by the voxel volume and the number of voxels in 100 g of tissue (Equation 2).

*Determination of the Infusion Protocol*

A biphasic infusion protocol was used to keep the blood iodine concentration level constant during the second CT data acquisition. This made the calculation of CBV based on a simple dilution principle valid, and eliminated the need for individual section calibration of intravascular concentration of contrast agent. The first phase of contrast infusion served as a loading dose. The second phase served as a maintenance dose and was tailored to match the redistribution/clearance kinetics of contrast agent from the blood. The maintenance dose rate was calculated by using estimates of the blood concentration of contrast agent present at the end of the loading dose phase, the total blood volume in the animal, and the average rate of change of contrast concentration in blood (11).

The blood concentration of contrast material present at the end of the loading dose phase ($C_0$) can be obtained by calculation, assuming homogeneous mixing within the total body blood pool. The theoretical value for $C_0$ is 16.2 mg/mL when we assume a blood volume of 70 mL/kg of lean body weight (12), a 20-second infusion at 35 mL/min, a 3-kg animal, and a concentration rate-of-change constant, $b_1$, of 0.02/s.

We measured $b_1$ experimentally in three animals as follows. Dynamic single-section data acquisition was begun before and continued during and after a 20-second infusion of contrast material at a rate of 35 mL/min for a total imaging time of 400 seconds. The imaging parameters for this dynamic study were those used for the 3-D functional CT studies, and the acquisition rate was one image every 5 seconds for the first 40 images, and one image every 10 seconds thereafter. Data were analyzed by the construction of a time-ΔHU blood curve, obtained from the common carotid arteries. A two-exponential model ($C = a_1 \cdot \exp[-b_1 \cdot t] + a_2 \cdot \exp[-b_2 \cdot t]$) was used to fit to the data from the point after cessation of infusion to the end of image acquisition (about 6 minutes). This portion of the curve showed changes in contrast agent concentration in the blood during initial redistribution and early elimination phases. The rate constants obtained were $b_1 = 0.021 \pm 0.002\ s^{-1}$ (mean ± SD), and $b_2 = 0.0018 \pm 0.0004\ s^{-1}$. To calculate the maintenance rate of infusion, only $b_1$ was used. This is because the contribution to concentration change from $b_2$ was less than 2% of the overall redistribution effect (dominated by $b_1$) during the 20 seconds of spiral imaging, allowing first-order kinetics to be used.

The infusion rate necessary to maintain a constant blood concentration of contrast material during the spiral acquisition depends on the actual achieved blood concentration after initial infusion (in this study about 16 mg of iodine per milliliter), the redistribution constant $b_1$ (0.021 $s^{-1}$), and the animal's blood volume ($V_{blood}$). The maintenance infusion rate (IR) as a function of these parameters is closely approximated by

$$3) \qquad IR = V_{blood} \cdot C_0 \cdot (1 - e^{-b_1 t}).$$

Figure 1A shows the relationship of infusion rate and varying $C_0$ values from this equation.

In the present study, which made use of iohexol with an iodine concentration of 350 mg/mL, the calculated maintenance infusion rate was 12.8 mL of iohexol 350/min. The closest rate allowed by our infusion pump was 12 mL/min, which we deemed acceptable. In two animals, the validity of the tailored infusion protocol was tested by collecting the dynamic data from a single section location during the biphasic infusion. One image was acquired every 5 seconds, with the same imaging parameters as those used for the spiral 3-D functional CT studies. An ROI was placed over the common carotid arteries, and a time-ΔHU curve created. Figure 1B shows the experimentally measured validation curves in these two animals. Only after the infusion protocol was determined and validated were the 3-D functional CT studies performed.

## Results

Blood decay constants and corresponding half-lives for each animal are presented in Table 1. The mean values of the measured decay constants, $b_1$ and $b_2$, were $0.021 \pm 0.002\ s^{-1}$ and $0.0018 \pm 0.0004\ s^{-1}$, with half lives of 0.54 ± 0.04 minute and 6.3 ± 1.3 minute, respectively. In two animals, the constancy of the blood concentration levels was demonstrated by using the experimental infusion scheme: these experimentally measured curves are shown in Figure 1B. The time at which the infusion rate changed is indicated by an arrow;

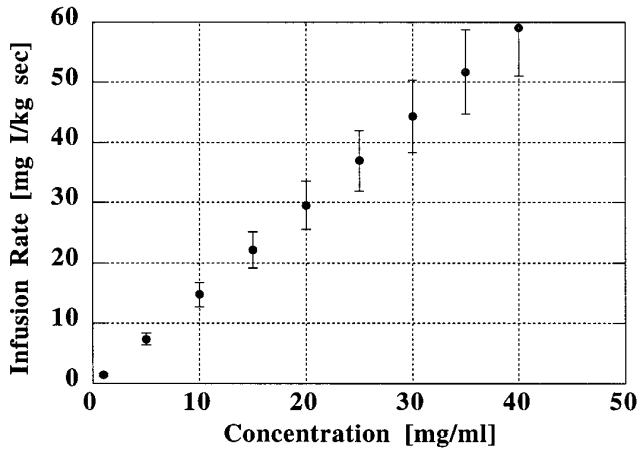


A

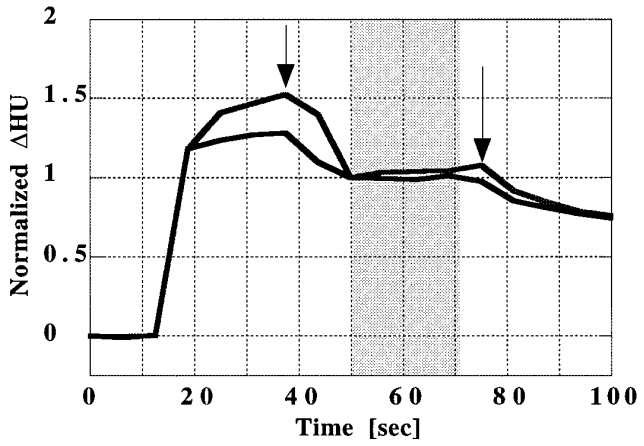


B

Fig 1. *A*, The infusion rate is presented as a function of initial concentration (immediately after the loading dose) in milligrams of iodine per kilogram of body weight and unit of time. The infusion rate in milliliters of iohexol per second can easily be calculated by multiplying the value by the body weight and dividing by the concentration (milligrams of iodine per milliliter) of the contrast agent.

*B*, Two experimentally measured infusion curves are presented. The first *arrow* corresponds to the change of the infusion rate, and the second *arrow* to the stoppage of infusion. Change of the infusion rate required approximately 5 seconds, which caused the concentration level to drop. A further 2-second delay before the actual start of the data collection was caused by the CT scanner. The *gray area* represents the time when the second spiral data acquisition would have taken place. Note the constant concentration level within this time, indicating that the maintenance dose selected is able to replace the cleared material.

the time interval corresponding to the course of the second 3-D functional CT data acquisition is marked by shading. The second arrow indicates the cessation of infusion, after which time the blood concentration begins to decay. Note the plateau in concentration during the period of spiral data acquisition.

The average CBV was determined to be 3.3 ± 0.5 mL/100 g. The values for individual animals are presented in Table 2. The regional blood volumes for the cortical gray matter, white matter, and basal ganglia were 4.5 ± 0.6 mL/100 g, 2.5 ± 0.6 mL/100 g, and 3.7 ± 0.4 mL/100 g, respectively. Figure 2 shows 3-D functional CT blood volume maps for one healthy animal at eight section locations. The major vessels are easy to identify and can therefore be excluded from the brain tissue blood volume analysis.

In the three ischemic animals, the distribution of the CBV deficit was consistent with the distribution of ischemia expected for this model (13). The hemispheric blood volumes on the side contralateral to ischemia were 3.8 ± 1.1 mL/100 g, 4.0 ± 1.1 mL/100 g, and 3.2 ± 1.1 mL/100 g. In the ischemic areas, the blood volumes were 1.5 ± 0.6 mL/100 g, 1.6 ± 0.8 mL/100 g, and 0.7 ± 1.1 mL/100 g, respectively. Figure 3 provides an example of the blood volume maps obtained in an ischemic animal. In this figure, the ischemic area can be clearly seen as an area of decreased blood volume. These results signify the feasibility of the 3-D functional CT technique as a tool with which to demonstrate intracerebral blood volume and thereby to measure the degree and extent of cerebral ischemia.

## Discussion

In the current investigation, we established that the subtraction 3-D functional CT technique is able to measure absolute regional blood volume in the brain. We demonstrated the usefulness of this technique as a tool with which to detect acute ischemia in affected areas of brain on the basis of decreased CBV in an animal model of focal ischemia. This subtraction 3-D functional CT study protocol can be performed rapidly, and the technique is easy to add to a conventional CT study. Subtraction 3-D functional CT yields important information about cerebrovascular pathophysiology that can be considered together with morphologic data in the diagnosis and treatment of patients.

The average CBV we obtained for rabbits (3.8 ± 0.6% or 3.3 ± 0.4 mL/100 g) is comparable to the values of CBV obtained in humans by using stimulated X-ray fluorescence (3.2 ± 0.94%) (14), conventional CT (3.0% with a range of 2.4% to 4.25%) (15), or single-photon emission CT (4.81 ± 0.37 mL/100 g brain)

**TABLE 1: Blood decay constants ($b_1$ and $b_2$) and corresponding half-lives ($T_{1/2}$) for each animal**

| Animal | 1/s | | min | |
|---|---|---|---|---|
| | $b_1$ | $b_2$ | $T_{1/2}$ | $T_{1/2}$ |
| 1 | 0.0200 | 0.0015 | 0.58 | 7.52 |
| 2 | 0.0211 | 0.0017 | 0.55 | 6.63 |
| 3 | 0.0229 | 0.0024 | 0.50 | 4.88 |
| Mean ± SD | 0.0214 ± 0.0015 | 0.0019 ± 0.0004 | 0.54 ± 0.04 | 6.34 ± 1.34 |

**TABLE 2: Total cerebral blood volume (CBV) and regional blood volumes for gray matter, white matter, and basal ganglia for each animal**

| Animal | CBV (mL/100 g of tissue) | | | |
|---|---|---|---|---|
| | Total Brain | Gray Matter | White Matter | Basal Ganglia |
| 1 | 3.4 ± 0.5 | 4.6 ± 0.3 | 2.6 ± 0.3 | 3.5 ± 0.5 |
| 2 | 4.6 ± 0.7 | 6.0 ± 0.7 | 3.4 ± 0.7 | 4.7 ± 0.6 |
| 3 | 2.7 ± 0.4 | 3.6 ± 0.5 | 1.8 ± 0.5 | 2.7 ± 0.4 |
| 4 | 2.6 ± 0.5 | 3.6 ± 0.5 | 1.8 ± 0.5 | 2.9 ± 0.4 |
| 5 | 4.5 ± 0.4 | 5.1 ± 0.7 | 3.1 ± 0.7 | 4.3 ± 0.4 |
| 6 | 3.5 ± 0.4 | 3.9 ± 0.6 | 2.1 ± 0.6 | 3.9 ± 0.3 |
| 7 | 1.9 ± 0.3 | 4.7 ± 0.8 | 2.8 ± 0.7 | 4.0 ± 0.3 |
| Mean ± SEM | 3.3 ± 0.4 | 4.5 ± 0.6 | 2.5 ± 0.6 | 3.7 ± 0.4 |

(16). Sklar et al (17) made use of a radionuclide technique to determine CBV in a cat model. They obtained a measure of 1.9 mL/100 g with $^{51}$Cr-labeled red cells as a marker, and a measure of 2.7 mL/100 g with radioiodinated serum albumin as a marker. In another study, researchers used a photoelectric method to measure 4.4% total CBV in cats (18). Independent researchers used a modification of this photoelectric technique to obtain a CBV measure of 4.8% in normal rats (19). Moreover, in an experimental stroke model using rats, T1-weighted magnetic resonance (MR) images were used to determine a hemispheric CBV measure of 3.4% ± 1.4%, contralateral to ischemia (20). In our own previous study of cerebral hemodynamics, we measured blood volume in normal New Zealand White rabbits by using first-pass functional CT. The values we obtained for cortical gray matter, white matter, and basal ganglia (4.3 ± 0.6 mL/100 g, 3.1 ± 0.4 mL/100 g, and 3.9 ± 0.5 mL/100 g, respectively) are practically identical to the CBV values obtained by using subtraction 3-D functional CT (4.5 ± 0.6 mL/100 g for cortical gray matter, 2.5 ± 0.6 mL/100 g for white matter, and 3.7 ± 0.4 mL/100 g for the basal ganglia) (5).

Despite the small size of the brain studied in our investigation (about 25 to 30 mm longitudinally, 24 mm transversely), the excellent spatial resolution afforded by 3-D functional CT permitted us to exclude the major vessels from the brain tissue ROI. For larger objects, such as the human brain, about 1-mm$^3$ voxels (240-mm field of view, 5-mm section thickness, and 512 × 512 image matrix) can routinely be obtained and will provide better tissue homogeneity than that seen in the brains of small animals. Owing to the high resolution of CT and the possibility for constructing overlapping sections from spiral raw data, we expect it to be feasible to measure relatively small areas of decreased blood volume in humans. In our study, the small size of the rabbit brain mandated thin-section, small-field-of-view imaging. The low signal-to-noise ratio that resulted was compensated for by increasing the dose of contrast agent used. In humans, the improved signal-to-noise ratio resulting from larger voxels will allow reduction of contrast loading to values conventionally used for head and neck CT angiography (~0.5 g of iodine per kilogram of body weight).

In the present work, we made an effort to achieve a constant blood concentration by replacing continually cleared contrast material through an infusion technique. If the blood concentration does alter, it can be measured from each image, and the image normalized by this value. For cases in which a slow, linear decay exists during the rapid spiral data acquisition, measurements made at the beginning and end of data collection are sufficient, and a correction

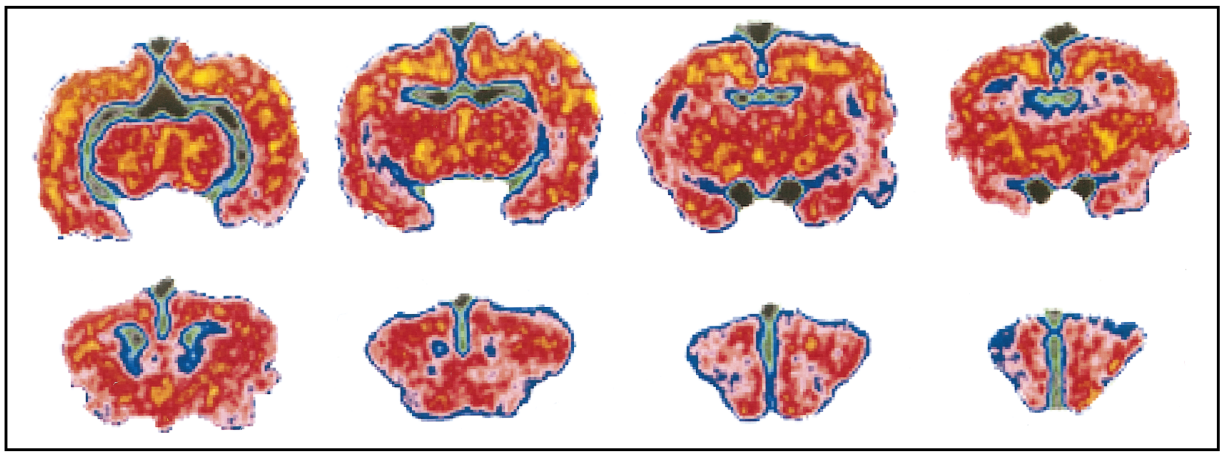

Fig 2. CBV maps of a healthy animal in eight consecutive coronal sections. These images, obtained in a rabbit brain, were produced by using the subtraction 3-D functional CT technique (section thickness = 2 mm).

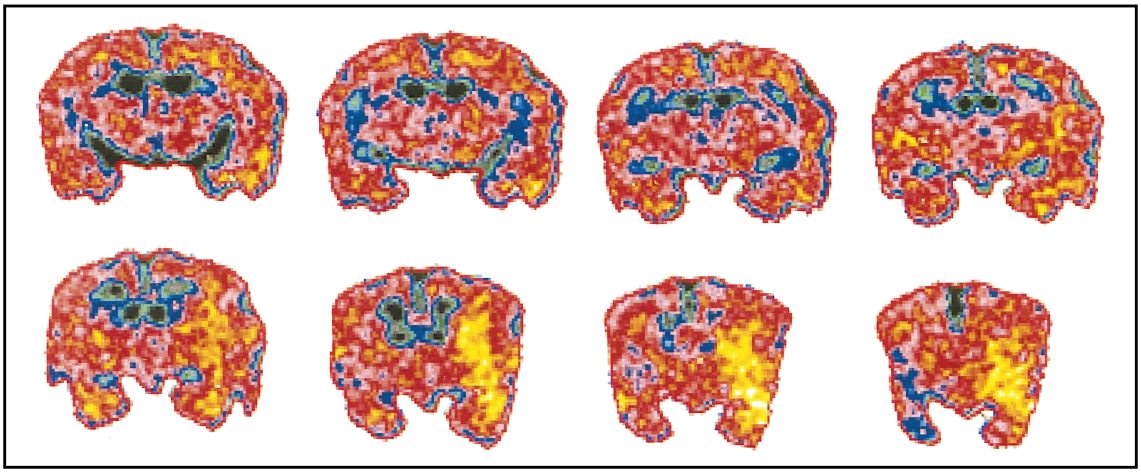

Fig 3. Eight maps of absolute blood volume at contiguous locations in a rabbit brain, measured with a subtraction 3-D functional CT technique and conventional iodine contrast material. Note the areas of low blood volume that correspond to the region of ischemia that had developed within 3 hours of middle cerebral artery occlusion (section thickness = 1 mm).

factor for each image can be easily calculated by interpolation to the known acquisition time for each image. Constant blood concentration could be achieved in clinical practice by adjusting the infusion protocol presented herein to the appropriate human body weight (see Fig 1). This can easily be done by modifying currently used CT angiography protocols to ensure a steady concentration of contrast material in the brain during image acquisition.

Motion and its elimination from the images will be a challenge in clinical imaging. On the basis of our preliminary experience, it is evident that the baseline and contrast-infusion spiral studies must be coregistered before subtraction and the calculation of CBV maps can be undertaken. We expect automated, volumetric registration algorithms to lead eventually to motion-free studies.

In clinical practice, it is common to obtain a CT examination for all patients thought to have brain ischemia before further treatment decisions are made. On the basis of a CT study, a sufficiently specific, underlying pattern of abnormality can be identified, allowing the distinction between embolic, hypotensive, or hemorrhagic causes (1). The aim of recent advances in interventional efforts has been to reduce the consequences of cerebrovascular insult (21). The time window for instituting appropriate treatment to help minimize neuronal deficits during ischemia is variable, but usually short,

often within a few hours after the ictus (22). Within this time, the degree and extent of the insult may be revealed by observation of patterns of perfusion deficit. We developed our subtraction 3-D functional CT technique in order to obtain this information through detection of absolute blood volume in the whole brain within a matter of minutes. As the method is quantitative and provides absolute measures, it can be used to follow the effects of the treatment, and comparisons between different patients and the same patients at different times become easy to obtain.

The 3-D functional CT technique provides a multiparametric study from an imaging examination that requires a relatively short study time. In addition to the conventional CT data for morphologic evaluation, 3-D functional CT can yield large-vessel angiograms as well as quantitative maps of absolute CBV. Angiographic and tissue perfusion images may be created off-line by image postprocessing, thus avoiding any significant increase in the actual study time. A CT angiogram may be produced by applying a maximum intensity projection algorithm to the subtraction data (23), whereas absolute blood volume maps may be obtained by using the methods presented in this article.

The blood-brain barrier, if intact, prevents extravasation of contrast material into the extravascular space, and thereby makes feasible the use of current, clinically approved iodine-based contrast agents for subtraction 3-D functional CT cerebral studies. However, in some pathologic situations, the blood-brain barrier may break down, allowing some contrast agent particles to pass into the extravascular space. Thus, the measurement of CBV becomes subject to error; generally, an overestimation of CBV occurs. Spiral CT technology, however, is able to acquire the data with considerable speed (a 3-D data acquisition of the whole brain requires about 30 seconds), so that the time for extravasation is minimal and any error caused by it is thus negligible. Earlier studies (CT and radionuclide brain scanning) have shown that impaired perfusion in the ischemic area delays the time at which contrast agent extravasation can be detected (24). For instance, Gado et al (24) have postulated that the lack of observable CT enhancement in brain infarction was the result of impaired perfusion and slow delivery of the contrast material in CT studies that were acquired after 4 minutes of contrast infusion. This finding supports our assumption that subtraction 3-D functional CT, because of its rapidity, is a valid method for studies of acute ischemia and infarction caused by impaired vascular function. These assumptions, however, are not valid for studies of other brain disorders, such as tumors, because of the marked morphologic irregularity of the vascular structure of tumors and the associated disruption of blood-brain barrier integrity (24).

Other imaging techniques that have been used to assess acute stroke without reliance on secondary information (such as edema) include first-pass functional CT as well as diffusion and perfusion MR imaging. The measurement of molecular diffusion processes by diffusion MR imaging has been shown to be a promising tool that can indicate acute ischemia in animal models within minutes of the onset of an insult (25–28). However, at present, diffusion MR imaging is not widely available in routine clinical practice, primarily because diffusion-weighted pulse sequences entail hardware requirements imposed by the large gradient strengths necessary to detect associated motion (27). Also, because the technique is sensitive to any motion, it is difficult to apply diffusion MR imaging to clinical practice without echo-planar capability, which is currently available only in a few institutions (29, 30).

Dynamic susceptibility contrast MR imaging, a bolus tracking method able to detect acute stroke on the basis of its primary cause, decreased perfusion (31–34), produces relative measures of cerebral hemodynamics in a single cerebral section (30–39). More recent improvements in echo-planar imaging have added multisection capability to MR imaging in those centers that have the requisite specialized hardware (40). Centers with conventional MR imagers may also obtain multiple sections by repeating the bolus injection of contrast agent and performing several data acquisitions. In addition, susceptibility contrast MR imaging can provide relative blood volume measurements by using a long-lived, intravascular contrast agent without rapid imaging (41).

Bolus-tracking functional CT provides high-resolution, quantitative maps of CBV, cerebral blood flow, and contrast agent transit and arrival times (5). This technique is currently limited to single-section studies for all except two commercial CT scanners. By repeating the bolus injection of contrast agent, however, multi-

ple sections may be studied. The benefits of the functional CT technique include its high spatial resolution (with 240-mm field of view, 5-mm section thickness, and 512 × 512 matrix size, voxel volume is 1 $mm^3$) and the absolute measures of hemodynamics it provides. Moreover, the temporal characterization of the concentration-time curves can be represented quite accurately by functional CT (5).

In purely clinical terms, we expect that CBV mapping alone may provide sufficient data with which to triage and treat a patient with acute stroke. Two 30-second spiral 3-D functional CT data acquisitions can allow us to obtain absolute blood volume through the whole brain sufficient to guide treatment. Further, the availability of the spiral CT technology necessary to perform these studies is already considerable, and increasing. In light of these considerations, we believe that quantitative subtraction 3-D functional CT has the potential to provide a rapid, simple, and cost-effective method for the study of acute and hyperacute stroke and other vascular pathophysiologies in the brain. Because the technique can be automated and made available on a 24-hour basis, 3-D functional CT has the potential to provide a valuable tool both for emergency evaluations of acute stroke and for those evaluations scheduled within routine radiologic practice. We believe that the subtraction 3-D functional CT technique will be highly valuable in clinical practice, as it provides 3-D measurement of cerebral microcirculation, expressed as blood volume, without introducing undue delay.

## Appendix

A correction factor for adjusting the difference between large and small cerebral vessel hematocrit was calculated as follows. Let $Hct_{WB}$ be the large-vessel hematocrit and $Hct_T$ be the hematocrit in brain capillaries. The ratio of small-vessel hematocrit to large-vessel hematocrit is 0.85 (ie, $Hct_T = 0.85 \cdot Hct_{WB}$) (42). We assume that the contrast agent is homogeneously mixed in the plasma space through the whole blood volume, yielding an equal concentration of contrast agent in large- and small-vessel plasma space. The ΔHU values represent concentrations in voxels that are either blood (red cells plus plasma) or tissue (extravascular space plus red cells plus plasma). These we mark as $C_{WB}$ and $C_T$, respectively. The concentration in the large vessel plasma, Cp, may be calculated by dividing the amount of contrast agent in the voxel ($C_{WB} V_{voxel}$) by that voxel's plasma volume, $V_{voxel}(1 - Hct_{WB})$:

$$1) \qquad C_p = \frac{C_{WB} V_{voxel}}{V_{voxel}(1 - Hct_{WB})}$$

The concentration of contrast agent in the capillary plasma can be calculated similarly:

$$2) \qquad C_p = \frac{C_T V_{voxel}}{f \cdot V_{voxel}(1 - Hct_T)},$$

where f is the fraction of blood in the tissue voxel. By making the right-hand sides of Equation 1 and Equation 2 equal and solving for the fractional blood volume, f, we get:

$$3) \qquad f = \frac{C_T(1 - Hct_{WB})}{C_{WB}(1 - Hct_T)}$$

The correction factor, CF, is obtained by converting $Hct_T$ so as to correspond to large-vessel hematocrit:

$$4) \qquad CF = \frac{1 - Hct_{WB}}{1 - 0.85 \cdot Hct_{WB}}$$

In the present study, the hematocrit was not measured in each animal. Instead, we used the average large-vessel hematocrit value of 36.3 ± 3.2 for the rabbits (43). The range of the large-vessel hematocrit for these animals was 29 to 43 (43), which corresponds to a range of correction factors from 0.89 to 0.94. In this study, the error in the calculated CBV values (caused by the use of an average hematocrit value) was less than 2% and ranged from 0.09 mL/100 g in gray matter to 0.05 mL/100 g in white matter.

## Acknowledgments

We thank Marek Trocha, Mary Teresa Shore, and Heni Kovach for their technical assistance in the course of the project. We also express our appreciation to JoAnne Fordham for her invaluable editorial help in preparing the manuscript.

## References

1. Gaston A, Thomas P, Valiente E, Chakir N, Combes C. Contribution of computerized tomography to the diagnosis of acute cerebral ischaemia. *J Neuroradiol* 1993;20:121–138
2. Marks MP, Napel S, Jordan JE, Enzmann DR. Diagnosis of carotid artery disease: preliminary experience with maximum-intensity projection spiral CT angiography. *AJR Am J Roentgenol* 1993; 160:1267–1271
3. Castillo M. Diagnosis of disease of the common carotid artery bifurcation: CT angiography vs catheter angiography. *AJR Am J Roentgenol* 1993;161:395–398
4. Schwartz RB. Neuroradiological applications of spiral CT. *Semin Ultrasound CT MRI* 1994;15:139–147
5. Hamberg LM, Hunter GJ, Halpern EF, Hoop B, Gazelle GS, Wolf GL. Quantitative, high resolution measurement of cerebrovascular physiology with slip-ring CT. *AJNR Am J Neuroradiol* 1996;17: 639–650
6. Pan Y, Lo EH, Matsumoto K, Hamberg L, Jiang H. Quantitative and dynamic MRI neuorprotection in experimental stroke. *J Neurol Sci* 1995;131:128–134

7. Lo EH, Steinberg GK, Panahian N, Maidment NT, Newcomb R. Profiles of extracellular amino acid changes in focal cerebral ischemia: effects of mild hypothermia. *Neurol Res* 1993;15:281–287
8. Lo EH, Steinberg GK. Effects of hypothermia on evoked potentials, magnetic resonance imaging and blood flow in focal ischemia in rabbits. *Stroke* 1992;23:889–893
9. Sabatini U, Celsis P, Viallard G, Rascol A, Marc-Vergens J-P. Quantitative assessment of cerebral blood volume by single-photon emission computed tomography. *Stroke* 1991;22: 324–330
10. Phelps ME, Grubb RL, Ter-Pogassian MM. Correlation between Pa(CO2) and regional cerebral blood volume by X-ray fluorescence. *J Appl Physiol* 1973;35:274–280
11. Goldstein A, Aronow L, Kalman SM. *Principles of Drug Action: The Basis of Pharmacology*. 2nd ed. New York, NY: Wiley; 1974:301–355
12. Guyton AC. The body fluid compartments: extracellular and intracellular fluids: interstitial fluid and edema. In: *Textbook of Medical Physiology*. 8th ed. Philadelphia, Pa: Saunders; 1991:273–285
13. Lo EH, Steinberg GK. Effects of dextromethorphan on regional cerebral blood flow in focal cerebral ischemia. *J Cereb Blood Flow Metab* 1991;11:803–809
14. Grubb RL, Phelps ME, Ter-Pogassian MM. Regional cerebral blood volume in humans. *Arch Neurol* 1973;28:38–44
15. Penn RD, Walser R, Ackerman L. Cerebral blood volume in man: computer analysis of a computerized brain scan. *JAMA* 1975; 234:1154–1155
16. Sakai F, Nakazawa K, Tazaki Y, et al. Regional cerebral blood volume and hematocrit measured in normal human volunteers by single-photon emission computed tomography. *J Cereb Blood Flow Metab* 1985;5:207–213
17. Sklar FH, Burke EF, Langfitt TW. Cerebral blood volume: values obtained with Cr51-labeled red blood cells and RISA. *J Appl Physiol* 1968;24:79–82
18. Tomita M, Gotoh F, Sato T, et al. Photoelectric method for estimating hemodynamic changes in regional cerebral tissue. *Am J Physiol* 1978;235:H56–H63
19. Sandor P, Cox-van Put J, de Jong W, de Wied D. Continuous measurement of cerebral blood volume in rats with the photoelectric technique: effect of morphine and naloxone. *Life Sci* 1986;39: 1657–1665
20. Kent TA, Quast MJ, Kaplan BJ, et al. Cerebral blood volume in a rat model of ischemia by MR imaging at 4.7 T. *AJNR Am J Neuroradiol* 1989;10:335–338
21. Marler JR. The National Institute of Neurological Disorders and Stroke rt-PA Stroke Study Group. Tissue plasminogen activator for acute ischemic stroke. *N Engl J Med* 1995;333:1581–1587
22. Siesjö BK. Pathophysiology and treatment of focal cerebral ischemia. *J Neurosurg* 1992;77:337–354
23. Napel S, Marks MP, Rubin GD, et al. CT angiography with spiral CT and maximum intensity projection. *Radiology* 1992;185:607–610
24. Gado MH, Phelps ME, Coleman RE. An extravascular component of contrast enhancement in cranial computed tomography. *Radiology* 1975;117:589–593
25. Moseley ME, Cohen Y, Mintorovitch J, et al. Early detection of regional cerebral ischemia in cats: comparison of diffusion- and T2-weighted MRI and spectroscopy. *Magn Reson Med* 1990;14: 330–346
26. Moseley ME, Kucharczyk J, Montorovitch J, et al. Diffusion-weighted MR imaging of acute stroke: correlation with T2-weighted and magnetic susceptibility-enhanced MR imaging in cats. *AJNR Am J Neuroradiol* 1990;11:423–429
27. LeBihan D. Molecular diffusion nuclear magnetic resonance imaging. *Magn Reson Q* 1991;7:1–30
28. Lo EH, Matsumoto K, Pierce AR, Garrido L, Luttinger D. Pharmacologic reversal of acute changes in diffusion-weighted magnetic resonance imaging in focal cerebral ischemia. *J Cereb Blood Flow Metab* 1994;14:597–603
29. Kwong KK, McKinstry RC, Chien D, Crawley AP, Pearlman JD, Rosen BR. CSF-suppressed quantitative single-shot diffusion imaging. *Magn Reson Med* 1991;21:157–163
30. Turner R. Single-shot diffusion imaging at 2.0 Tesla. *J Magn Reson* 1990;86:445–452
31. Warach S, Li W, Ronthal M, Edelman RR. Acute cerebral ischemia: evaluation with dynamic contrast-enhanced MR imaging and MR angiography. *Radiology* 1992;182:41–47
32. Hamberg LM, MacFarlane R, Tasdemiroglu E, et al. Measurement of cerebrovascular changes in cats after transient ischemia using dynamic magnetic resonance imaging. *Stroke* 1993;24:444–450
33. Kucharczyk J, Vexler ZS, Roberts TP, et al. Echo-planar perfusion-sensitive MR imaging of acute cerebral ischemia. *Radiology* 1993;188:711–717
34. Maeda M, Itoh S, Ide H, et al. Acute stroke in cats: comparison of dynamic susceptibility-contrast MR imaging with T2- and diffusion-weighted MR imaging. *Radiology* 1993;189:227–232
35. Rosen BR, Belliveau JW, Vevea JM, Brady TJ. Perfusion imaging with NMR contrast agents. *Magn Reson Med* 1989;249–265
36. Edelman RR, Mattle HP, Atkinson DJ, et al. Cerebral blood flow: assessment with dynamic contrast-enhanced T2*-weighted MR imaging at 1.5T. *Radiology* 1990;176:211–220
37. Dean BL, Lee C, Kirsch JE, Runge VM, Dempsey RM, Pettigrew LC. Cerebral hemodynamics and cerebral blood volume: MR assessment using gadolinium contrast agents and T1-weighted turbo-FLASH imaging. *AJNR Am J Neuroradiol* 1992;13:39–48
38. Perman WH, El-Ghazzaway O, Gado MH, Larson KB, Perlmutter JS. A half-Fourier gradient echo technique for dynamic MR imaging. *Magn Reson Imaging* 1993;11:357–366
39. Rempp KA, Brix G, Wenz F, Becker CR, Gü ckel F, Lorenz WJ. Quantitation of regional cerebral blood flow and volume with dynamic susceptibility contrast-enhanced MR imaging. *Radiology* 1994;193:637–641
40. Aronen HJ, Gazit IE, Louis DN, et al. Cerebral blood volume maps of gliomas: comparison with tumor grade and histologic findings. *Radiology* 1994;191:41–51
41. Hamberg LM, Boccalini P, Stranjalis G, et al. Continuous assessment of cerebral blood volume in transient ischemia using steady state susceptibility-contrast MRI. *Magn Reson Med* 1996;35:168–173
42. Phelps ME, Grubb RL, Ter-Pogassian MM. In vivo regional cerebral blood volume by X-ray fluorescence: validation of method. *J Appl Physiol* 1973;35:741–747
43. Weisbroth SH, Flatt RE, Kraus AL. *The Biology of the Laboratory Rabbit.* New York, NY: Academic Press; 1974:68